

Components of near-surface energy balance derived from satellite soundings

K. Mallick et al.

This discussion paper is/has been under review for the journal Biogeosciences (BG).  
Please refer to the corresponding final paper in BG if available.

# Components of near-surface energy balance derived from satellite soundings – Part 1: Net available energy

K. Mallick<sup>1</sup>, A. Jarvis<sup>2</sup>, G. Wohlfahrt<sup>3</sup>, G. Kiely<sup>4</sup>, T. Hirano<sup>5</sup>, A. Miyata<sup>6</sup>, S. Yamamoto<sup>7</sup>, and L. Hoffmann<sup>1</sup>

<sup>1</sup>Department of Environment and Agro-biotechnologies, Centre de Recherche Public – Gabriel Lippmann, L4422, Luxembourg

<sup>2</sup>Lancaster Environment Centre, Lancaster University, LA1 4YQ, UK

<sup>3</sup>Ecosystem Research & Landscape Ecology, University of Innsbruck, 6020 Innsbruck, Austria

<sup>4</sup>Hydrometeorology Research Group, Department of Civil and Environmental Engineering, University College Cork, Ireland

<sup>5</sup>Division of Environmental Resources, Research Faculty of Agriculture, Hokkaido University, Hokkaido, Japan

<sup>6</sup>National Institute for Agro-Environmental Sciences, Tsukuba, Japan

<sup>7</sup>Graduate School of Environmental Science, Okayama University Tsushimanaka 3-1-1, Okayama 700-8530, Japan

Title Page

Abstract

Introduction

Conclusions

References

Tables

Figures



Back

Close

Full Screen / Esc

Printer-friendly Version

Interactive Discussion



Received: 27 March 2014 – Accepted: 23 July 2014 – Published: 6 August 2014

Correspondence to: K. Mallick (mallick@lippmann.lu)

Published by Copernicus Publications on behalf of the European Geosciences Union.

**BGD**

11, 11825–11861, 2014

**Components of near-surface energy balance derived from satellite soundings**

K. Mallick et al.

Title Page

Abstract

Introduction

Conclusions

References

Tables

Figures



Back

Close

Full Screen / Esc

Printer-friendly Version

Interactive Discussion



## Abstract

This paper introduces a relatively simple method for recovering global fields of near-surface net available energy (the sum of the sensible and latent heat flux or the difference between the net radiation and surface heat accumulation) using satellite visible and infra-red products derived from the AIRS (Atmospheric Infrared Sounder) and MODIS (MODerate Resolution Imaging Spectroradiometer) platforms. The method focuses on first specifying net surface radiation by considering its various shortwave and longwave components. This was then used in a surface energy balance equation in conjunction with satellite day–night surface temperature difference to derive 12 h discrete time estimates of surface, system heat capacity and heat accumulation, leading directly to retrieval for surface net available energy. Both net radiation and net available energy estimates were evaluated against ground truth data taken from 30 terrestrial tower sites affiliated to the FLUXNET network covering 7 different biome classes. This revealed a relatively good agreement between the satellite and tower data, with a pooled root mean square deviation of 98 and  $72 \text{ W m}^{-2}$  for net radiation and net available energy, respectively, although both quantities were underestimated by approximately 25 and 10 %, respectively relative to the tower observations. Analysis of the individual shortwave and longwave components of the net radiation revealed the downwelling shortwave radiation to be the main source of this systematic underestimation.

## 1 Introduction

An important manifestation of climate change is widespread alteration of the composition of the energy balance at the Earth's surface (Trenberth et al., 2009; Wild et al., 2013). Given the importance of being able to predict the consequences of climate change, both measurement and modelling of the components of surface energy balance attract significant attention from a broad range of related scientific disciplines

### Components of near-surface energy balance derived from satellite soundings

K. Mallick et al.

Title Page

Abstract

Introduction

Conclusions

References

Tables

Figures



Back

Close

Full Screen / Esc

Printer-friendly Version

Interactive Discussion



(Stephens et al., 2012). Two such disciplines are hydrology and meteorology, which share a common interest in resolving the balance between sensible,  $H$ , and latent,  $\lambda E$ , heat fluxes over a broad range of spatial and temporal scales (Anderson et al., 2012).

Net available energy,  $\Phi$ , is a core variable used to predict the magnitude of  $H$  and  $\lambda E$  given it is defined as the sum of these two fluxes (Wright et al., 1992; Migletta et al., 2009; Anderson et al., 2012),

$$\lambda\Phi = E + H \quad (1)$$

The utility of this definition arises from being able to also specify  $\Phi$  as the difference between the net broadband radiation,  $R_N$ , and the rate of heat accumulation,  $G$ , below the plain across which  $R_N$  is specified,

$$\Phi = R_N - G \quad (2)$$

Given  $R_N$  is routinely measured using net radiometers this affords an opportunity to specify  $\Phi$  and hence either  $H$  or  $\lambda E$ . For example, in modelling studies  $\lambda E$  is invariably specified as a function of  $\Phi$  using the ubiquitous equations such as those of Penman (1948) for open water or Monteith (1965) for land surfaces (Mu et al., 2011; Mallick et al., 2014a). Despite being the rate of change of heat stock in terrestrial environments,  $G$  is often interpreted as the “ground heat flux” and attempts to measure this using heat flux plates are commonplace (Mayocchi and Bristow, 1995; Sauer and Horton, 2005; Heitman et al., 2010). These measurements prove somewhat less reliable than  $R_N$  due to greater spatial heterogeneity in ground heat uptake (Gao et al., 1998; Tittebrand and Berger, 2009; Verhoef et al., 2012) allied to the fact that significant heat capacity resides in other elements of the land surface (Ochsner et al., 2007). As a result,  $G$  proves problematic in surface energy balance studies and is either ignored (Foken et al., 2006; Foken, 2008) or treated somewhat superficially (Choudhury, 1987), despite being significant under a broad range of conditions (Santanello and Friedl, 2003; Ochsner et al., 2007). Large scale estimates of  $G$  are useful in the context of regional and global evapotranspiration modelling and for verification of regional and Global Circulation Models (Kergoat et al., 2011).

**Components of near-surface energy balance derived from satellite soundings**

K. Mallick et al.

Title Page

Abstract

Introduction

Conclusions

References

Tables

Figures

◀

▶

◀

▶

Back

Close

Full Screen / Esc

Printer-friendly Version

Interactive Discussion





for use in a simple Bowen ratio  $\lambda E$  specification framework as detailed in a companion paper by Mallick et al. (2014b). Taking advantage of the extensive network of terrestrial eddy covariance tower sites (Baldocchi et al., 2001) which record direct measurements of  $R_N$ ,  $H$  and  $\lambda E$ , we use these measurements to derive independent non-radiative estimates of  $\Phi$  in order to critically evaluate our satellite estimates of this quantity.

## 2 Methodology

### 2.1 Net radiation

The approach for estimating  $R_N$  uses the Atmospheric Infrared Sounder (AIRS) radiation products, although we have also made use of the MODIS surface reflectance and solar zenith angle products where necessary.  $R_N$  is generated by considering the following balance between net shortwave ( $R_{NS}$ ) and longwave ( $R_{NL}$ ) radiation at or near the Earth's surface,

$$R_N = R_{NS} + R_{NL} = (1 - \alpha)R_{S\downarrow} + R_{L\downarrow} - R_{L\uparrow} \quad (3)$$

where  $\alpha$  is the surface albedo and  $R_{L\downarrow}$  and  $R_{L\uparrow}$  are the downwelling and upwelling thermal radiative fluxes and  $R_{S\downarrow}$  is the downwelling shortwave radiative flux (all fluxes specified in  $W m^{-2}$ ). Our chosen reference level for  $R_N$  is the near surface given this corresponds to the flux-based tower estimates we used in the evaluation. Therefore, surface  $R_{S\downarrow}$  was estimated from its top-of-atmosphere clear sky counterpart  $R_{SO\downarrow}$  and AIRS cloud cover fraction ( $f$ ) following Hildebrandt et al. (2007),

$$R_{S\downarrow} = (1 - f)\tau_A R_{SO\downarrow} \quad (4)$$

where  $\tau_A$  is the clear sky transmissivity of the atmosphere which we assume is 0.75 (Cano et al., 1986; Thornton and Running, 1999; Hildebrandt et al., 2007; Gubler et al., 2012). Although clearly a simplification, a constant clear sky transmissivity is widely

**BGD**

11, 11825–11861, 2014

## Components of near-surface energy balance derived from satellite soundings

K. Mallick et al.

Title Page

Abstract

Introduction

Conclusions

References

Tables

Figures

◀

▶

◀

▶

Back

Close

Full Screen / Esc

Printer-friendly Version

Interactive Discussion



used (e.g. Massaquoi, 1988; Bindi et al., 1992; Choudhury, 2001; Hildebrandt et al., 2007; Mallick et al., 2009) in recognition of the absence of robust alternatives. In addition, exploiting the AIRS cloud cover fraction data in Eq. (4) should help accommodate the effects of variations in both the aerosol optical depth (Kaufman and Koran, 2006; Quass et al., 2010) and atmospheric water vapor (Adhikari et al., 2006).

The terrestrial surface albedo was generated using the MODIS Aqua–Terra surface reflectances  $r_i$  following Liang et al. (1999),

$$\alpha = \sum_{i=1}^N p_i r_i + 0.0036 \quad (5)$$

where  $r_i$  are the mid-point reflectances within the 0.62–0.67; 0.841–0.876; 0.459–0.479; 1.230–1.250; 1.628–1.653; 1.628–1.653; and 2.105–2.155  $\mu\text{m}$  wavelength bands and  $p_i$  are the weightings for each wavelength bands taken as  $p_i = [0.3973; 0.2382; 0.3489; -0.2655; 0.1604; -0.0138; 0.0682]$  (Liang et al., 1999, 2002). The albedo of the ocean varies according to the cosine of solar zenith angle (Jin et al., 2004). In the present case, a constant albedo of 0.04 was assumed for oceans given the satellite radiances are nadir.

Many of the longwave components of the radiative balance are very closely related to the raw IR radiances being measured by AIRS. Given these are not in the public domain we have attempted to recover them as follows, although in future we would anticipate using the raw IR radiances more directly if possible.  $R_{\text{NL}}$  was calculated as,

$$R_{\text{NL}} = R_{\text{L}\downarrow} - R_{\text{L}\uparrow} = \varepsilon_{\text{C}} \varepsilon_{\text{S}} \sigma T_{\text{C}}^4 - \varepsilon_{\text{S}} \sigma T_{\text{S}}^4 \quad (6)$$

where  $\sigma$  is the Stefan–Boltzmann constant ( $5.67 \times 10^{-8} \text{ W m}^{-2} \text{ K}^{-4}$ ),  $T_{\text{C}}$  is the columnar air temperature, and  $\varepsilon_{\text{C}}$  and  $\varepsilon_{\text{S}}$  are the column and surface emissivities. Among the different schemes for calculating  $\varepsilon_{\text{C}}$  we have used the formulation proposed by Prata (1996) given this appears to be the most reliable (Niemela et al., 2001; Bisht and Bras,

## BGD

11, 11825–11861, 2014

### Components of near-surface energy balance derived from satellite soundings

K. Mallick et al.

Title Page

Abstract

Introduction

Conclusions

References

Tables

Figures

◀

▶

◀

▶

Back

Close

Full Screen / Esc

Printer-friendly Version

Interactive Discussion



2010, 2011). This scheme uses AIRS total precipitable water ( $\xi$ ) information to estimate  $\varepsilon_C$  as,

$$\varepsilon_C = 1 - (1 + \xi)e^{-(1.2+3\xi)^{0.5}} \quad (7)$$

The columnar air temperature  $T_C$  in Eq. (6) is taken as the average of the 2 m and 1000 hPa pressure level AIRS temperatures in an attempt to reflect a weighting toward the lower troposphere when specifying  $R_{L\downarrow}$ .  $T_S$  and  $\varepsilon_S$  are taken directly from the AIRS skin temperature and surface emissivity products.

## 2.2 Surface heat capacity, ground heat flux and net available energy

The definition of  $G$  stems from consideration of the non-steady state surface energy balance,

$$c \frac{dT_S(t)}{dt} = R_N(t) - \lambda E(h) - H(t) = G(t) \quad (8)$$

where  $c$  is the aggregate surface system heat capacity. The AIRS sounder platform samples twice daily at 01:30 and 13:30 hours local time (LT). Despite being somewhat coarse, taking a discrete time, backward difference approximation of Eq. (8) with a sample interval of  $\Delta t = 12$  h equivalent to that of the AIRS pass gives,

$$\Delta T_S(t) = b_1 R_N(t) + b_2 \quad (9)$$

where  $\Delta T_S$  is the day–night surface temperature change,  $b_1 = \Delta t/c$  and  $b_2 = -\Phi(t)\Delta t/c$ . If we assume that the system is approximately in equilibrium over a 24 h cycle, and that at 01:30 LT  $\Phi \approx 0$  (for all 30 sites analysed in this study  $\Phi(01:30) < 0.05\Phi(13:30)$ ; see also Tamai et al., 1998; Mamadou et al., 2014), then this gives the following simultaneous equations:

$$\Delta T_S(13:30) = b_1 R_N(13:30) + b_2 \quad (10a)$$

$$-\Delta T_S(13:30) = b_1 R_N(01:30) \quad (10b)$$

Title Page

Abstract

Introduction

Conclusions

References

Tables

Figures

⏪

⏩

◀

▶

Back

Close

Full Screen / Esc

Printer-friendly Version

Interactive Discussion









the change in output per unit change in input, normalised by the median value of each. Only absolute sensitivities  $> 0.1$  were considered significant. The standard deviation of the estimated distributions of  $G$ ,  $R_N$  and  $\Phi$  were used as the summary statistic for the measurement uncertainty of the proposed methodology.

## 2.5 Evaluation of $R_N$ and $\Phi$

To evaluate the satellite values of  $R_N$  and  $\Phi$  we have made use of the extensive FLUXNET terrestrial tower network (Baldocchi et al., 2001). Clearly, there is a scale conflict here with the satellite retrievals being  $1^\circ$  whilst the individual tower observations are for scales of the order of 1 km or less. The tower  $R_N$  are from the broadband net radiometer sensors located on each tower. In the absence of reliable measures of  $G$  at the tower scale and in order to derive genuinely independent measures of  $\Phi$  against which to evaluate the satellite data, we have taken the tower net available energy as the sum of the measured sensible and latent heat flux i.e. Eq. (1). Thereby we have assumed that the eddy covariance flux measurements are able to close the energy balance (i.e.  $R_N - G = \lambda E + H$ ), the implications of which will be discussed below. We have chosen 30 sites covering a broad range of geographical locations selected from 7 land cover types including; evergreen broadleaf forest (EBF), mixed forest (MF), evergreen needle forest (ENF), deciduous broadleaf forest (DBF), savanna (SAV), grassland (GRA) and cropland (CRO). A comprehensive list of the site characteristics are provided in Table 1. Each tower evaluation dataset is comprised of the 13:30 LT samples of  $R_N$ ,  $H$  and  $\lambda E$  which correspond with the satellite overpass. Again, the evaluation is based on pooling these data into weighted monthly average values. For the evaluation we have elected to compare all 12 months of data for 2003 given this had the best overlap between the FLUXNET and AIRS databases.

# BGD

11, 11825–11861, 2014

## Components of near-surface energy balance derived from satellite soundings

K. Mallick et al.

Title Page

Abstract

Introduction

Conclusions

References

Tables

Figures

◀

▶

◀

▶

Back

Close

Full Screen / Esc

Printer-friendly Version

Interactive Discussion



### 3 Results

Table 2 shows the results from the sensitivity analysis. For  $G$  we see the importance of the long wave specification and in particular  $\varepsilon_C$ . The standard deviation of the estimate of  $G$  from the ensemble is  $18 \text{ W m}^{-2}$  giving approximate 95 % confidence detection limits of  $\pm 36 \text{ W m}^{-2}$  on the estimates.  $R_N$  is sensitive to all components of the radiation balance calculation as expected (Table 2). The standard deviation of the estimate of  $R_N$  from the ensemble is  $40 \text{ W m}^{-2}$  giving approximate 95 % detection limits of  $\pm 80 \text{ W m}^{-2}$  on the estimates (Table 2). Not surprisingly the sensitivity results for  $\Phi$  mirror those of  $R_N$  albeit with a marginally higher ensemble standard deviation of  $44 \text{ W m}^{-2}$  (Table 2).

The locations of the 30 terrestrial evaluation sites are marked in Fig. 1. Figure 2 shows annual average, global satellite scenes for 13:30 LT  $R_N$ ,  $c$ ,  $G$  and  $\Phi$  for 2003. Missing data in the images are mainly due to missing data in the AIRS soundings at high latitudes or over the mountain belts where it is difficult to profile air temperature and relative humidity reliably. In addition, persistent cloudy conditions also prevent reliable retrieval and hence are rejected although these will be less evident in the monthly or annual average data.

Figure 2a shows the global distribution of  $R_N$  which generally decreases with latitude as expected.  $R_N$  also decreases over land due to the generally higher albedo resulting in reduced absorption of the net shortwave radiation (Giambelluca et al., 1997; Gao and Wu, 2014) or relatively higher surface temperature increasing the net longwave component, especially over the drier regions (Liang et al., 1998; Trenberth, 2011). As a result the magnitude of  $R_N$  was around  $200\text{--}300 \text{ W m}^{-2}$  over the dry desert regions whereas the oceanic values of  $R_N$  were  $450\text{--}700 \text{ W m}^{-2}$ .

Figure 2b shows the global distribution of  $c$  (surface heat capacity). The oceanic values of  $4$  to  $8 \text{ MJ m}^{-2} \text{ K}^{-1}$  are equivalent to  $1$  to  $2 \text{ m}$  of sea water, which appears reasonable on the daily time step to which they relate (Stramma et al., 1986; Schwartz, 2007). These oceanic values are somewhat noisy due to the small day–night temperature differences observed for the oceans giving a relatively poor signal to noise ratio.

**BGD**

11, 11825–11861, 2014

## Components of near-surface energy balance derived from satellite soundings

K. Mallick et al.

Title Page

Abstract

Introduction

Conclusions

References

Tables

Figures

◀

▶

◀

▶

Back

Close

Full Screen / Esc

Printer-friendly Version

Interactive Discussion



## Components of near-surface energy balance derived from satellite soundings

K. Mallick et al.

Title Page

Abstract

Introduction

Conclusions

References

Tables

Figures



Back

Close

Full Screen / Esc

Printer-friendly Version

Interactive Discussion



However, behind this noise the pattern of oceanic  $c$  appears relatively uniform as one might expect. Over land  $c$  varies between 0.05–0.5 MJ m<sup>-2</sup> K<sup>-1</sup> with wetter tropical and high latitude areas showing significantly higher values than the drier, less vegetated areas as expected. The soil equivalent depth of this heat capacity is approximately 0.01 m, which again appears reasonable for a daily time step (Li and Islam, 1999), although in heavily vegetated areas  $c$  is obviously comprised of a more complex aggregation.

Figure 2c shows the global distribution of  $G$ . These are the 13:30 LT values, hence being net positive as an annual average. Between 20° N–S  $G$  is approximately 10 to 20 % of  $R_N$ , and this rises to more than 40 % above 50° N–S (Hsieh et al., 2009). Given this opposes the pattern of  $R_N$  one would conclude either some deficiencies in the way  $G$  is specified here or that  $R_N$  partitions into latent heat far more effectively than surface heating in these warm wet environments (Liu et al., 2005). Again, terrestrial values are lower than their oceanic equivalents mainly due to the lower heat capacity as well as reduced  $R_N$  as discussed above. This also highlights the role of the vegetation layer in preventing ground heating (Baker and Baker, 2002; Bounoua et al., 2010). The Sahara appears particularly prominent in this scene with high rates of midday heat accumulation which appears to be associated with a combination of moderate net radiation and relatively high heat capacity. The heterogeneity in this region appears to be related to the pattern of bare darker rock.

Figure 2d shows the global distribution of  $\Phi$  which follows a similar pattern to  $R_N$  as expected, although the pattern of  $G$  shown in Fig. 2c dictates that the N–S gradients in  $\Phi$  are somewhat stronger than those of  $R_N$ . Before discussing these results we consider their evaluation. Figure 3a shows the pooled evaluation of  $R_N$  which produced an overall correlation of  $r = 0.88 (\pm 0.03)$ <sup>1</sup>. Assuming both tower and satellite observations are linearly related through some “true” value, then the pooled values are co-related by  $R_N(\text{satellite}) = 0.75 (\pm 0.02) R_N(\text{tower}) + 23.37 (\pm 8.20)$  i.e. a small but significant underestimation in  $R_N$  (satellite) relative to  $R_N$  (tower). The root mean square

<sup>1</sup>All uncertainties are expressed as  $\pm$  one standard deviation unless otherwise stated.



## Components of near-surface energy balance derived from satellite soundings

K. Mallick et al.

Title Page

Abstract

Introduction

Conclusions

References

Tables

Figures



Back

Close

Full Screen / Esc

Printer-friendly Version

Interactive Discussion



to be  $58\text{--}142\text{ W m}^{-2}$  and  $37\text{--}40\text{ W m}^{-2}$  over South east Asia and China, respectively, using MODIS terra data products. Stackhouse et al. (2000) evaluated the International Satellite Cloud Climatology Project (ISCCP) data to have errors in the range 10 to  $15\text{ W m}^{-2}$  in monthly average shortwave and longwave radiative fluxes. When these errors are compounded in the derivation of  $R_N$  and compared with tower data, an RMSD of the order of  $98\text{ W m}^{-2}$  appears reasonable considering the spatial resolution of the AIRS data ( $1^\circ \times 1^\circ$ ).

There have been very few attempts to retrieve satellite estimates of  $\Phi$  and compare these with ground truth data, although the statistics from our attempt appear to parallel results of Stisen et al. (2008) who studied a single site in the Senegal River basin using 5 km spatial resolution MSG (Meteosat Second Generation) geostationary satellite data and obtained a correlation of  $r = 0.51$  and an RMSD of 14 to 17 % of the mean in comparison to the surface measurements.

As seen in Fig. 3a there is a systematic underestimation of  $R_N$  relative to the tower values which exceeds the typical accuracy of net radiometer measurements of  $20\text{ W m}^{-2}$  quoted by Foken (2008). We examined this underestimation in more detail wherever possible, by evaluating three of the individual radiation components of  $R_N$  ( $R_{S\downarrow}$ ,  $R_{L\downarrow}$  and  $R_{L\uparrow}$ ). All tower sites provided measurements of  $R_{S\downarrow}$  (but not  $R_{S\uparrow}$ ). Figure 3c shows  $R_{S\downarrow}$  is systematically underestimated at the satellite scale with  $R_{S\downarrow}(\text{satellite}) = 0.70 (\pm 0.02) R_{S\downarrow}(\text{tower}) + 68 (\pm 12.24)$  which accounts for the mismatch of  $R_N(\text{satellite}) \approx 0.75 R_N(\text{tower})$ . Before attempting to account for the various reasons for this underestimation it is important to realise that, unlike the IR components, the shortwave components are all-sky retrievals i.e. like the tower data they do not omit cloudy sky conditions. As a result, any bias in the shortwave is not as a result of biased sampling when comprising the monthly average. Besides, the omission of non-clear sky data would tend to lead to  $R_{S\downarrow}(\text{satellite}) > R_{S\downarrow}(\text{tower})$ .

If we assume  $\tau_A$  to be the principal reason for  $R_{S\downarrow}(\text{satellite}) < R_{S\downarrow}(\text{tower})$  then a global value of 0.75 would be, on average, too low. Given the relatively well defined relationship between  $R_{S\downarrow}(\text{satellite})$  and  $R_{S\downarrow}(\text{tower})$  seen in Fig. 3c one would imagine

## Components of near-surface energy balance derived from satellite soundings

K. Mallick et al.

Title Page

Abstract

Introduction

Conclusions

References

Tables

Figures

◀

▶

◀

▶

Back

Close

Full Screen / Esc

Printer-friendly Version

Interactive Discussion



that a more sophisticated dynamic representation of  $\tau_A$  would offer only marginal improvements. Recalibration of  $\tau_A$  using the tower data is a possibility although we have avoided this given the AIRS cloud cover fraction and scale mismatch between the satellite and tower could also be implicated in the observed bias. For example, the diffuse fraction of  $R_{S\downarrow}$ (tower) can become enriched by surface reflected solar radiation, particularly in undulating terrain (Dubayah and Loechel, 1997; Sultan et al., 2014). Nonlinear scaling effects of surface albedo (Oliphant et al., 2003; Salomon et al., 2006) can also be implicated in this because surface albedo interacts nonlinearly with surface characteristics such as surface wetness and land surface temperature (Ryu et al., 2008) or the leaf area index (Hammerle et al., 2008).

To probe the specification of  $R_N$  further we investigated the individual longwave radiation components in relation to measures of these fluxes available for a limited subset (14) of tower sites. From Fig. 3d and e it appears that there is quite good agreement between the satellite and tower data for both  $R_{L\downarrow}$  and  $R_{L\uparrow}$  and that any mismatch is insufficient to explain the discrepancy in  $R_N$ . This is somewhat surprising for two reasons. Firstly, unlike the shortwave component,  $R_L$ (tower) is all sky whilst  $R_L$ (satellite) is only from clear sky conditions where IR retrieval is possible. As a result, one would anticipate very significant differences in the monthly average values of the longwave components. However, it is difficult to predict the effect of this biased sampling on  $R_{NL}$ (satellite) given that cloud interacts with both  $R_{L\downarrow}$  and  $R_{L\uparrow}$  in complex ways. Secondly, one would anticipate significant scaling effects from the  $T^4$  nonlinearity in Eq. (6) which can result in a disproportionate contribution of warmer elements within the system to both  $R_{L\downarrow}$  and  $R_{L\uparrow}$  (Kustas and Norman, 2000; Lakshmi and Zehrhuhs, 2002; Corbari et al., 2010). The fact that these effects are not seen to any significant degree could point to compensating errors in the analysis but does not distract from the central message of the importance of the bias in the shortwave when accounting for  $R_N$ (satellite) <  $R_N$ (tower).

Figure 3b and Table 3 show that  $\Phi$ (satellite)  $\approx$  0.90 $\Phi$ (tower) suggesting a slight compensation for the underspecification of  $R_{S\downarrow}$  through the underspecification of  $G$  from the



## Components of near-surface energy balance derived from satellite soundings

K. Mallick et al.

Title Page

Abstract

Introduction

Conclusions

References

Tables

Figures

◀

▶

◀

▶

Back

Close

Full Screen / Esc

Printer-friendly Version

Interactive Discussion



satellite data. However, this evaluation assumes the energy balance to be closed in the tower data (i.e.  $R_N - G = \lambda E + H$ ), which typically is not the case,  $\lambda E + H$  often falling short of  $R_N - G$  by 20 % (Wilson et al., 2002). Because the causes of this energy imbalance remain controversial (see Foken, 2008 for review), it is difficult to estimate how much the tower values of  $\lambda E + H$  are actually biased low and hence the extent to which this bias affects our evaluation. The errors in the tower data are believed to be associated with different footprint characteristics for the different instruments used (Lin et al., 2008). For example,  $R_N$  observations typically have a footprint size of  $\sim 10 \text{ m}^2$  whilst air properties (e.g. air temperature, humidity) have footprint sizes of  $> 1 \text{ km}^2$ . By way of illustration, if, in the worst case, the entire energy imbalance was to be attributed exclusively to  $\lambda E + H$  (i.e.  $R_N - G$  are quantified correctly), then the true midday  $\lambda E + H$  could be some 20 % greater (Wilson et al., 2002). As a result, the present bias seen in Table 3 would change to  $\Phi(\text{satellite}) \approx 0.72\Phi(\text{tower})$  again implicating  $R_{\text{S}\downarrow}$  as the main source of bias in the satellite retrievals for both  $R_N$  and  $\Phi$ .

The method we present here for estimating  $R_N$  contrasts with more sophisticated model-based approaches which attempt to accommodate the complexity of atmospheric radiative transfer explicitly (e.g. Fouquart and Bonnel, 1980; Mlawer et al., 1997; Bisht and Bras, 2010; Hou et al., 2014). There are several reasons for adopting this stance. Firstly, the estimates of  $R_N$  need to be sympathetic with the simple dynamic energy balance used to accommodate  $G$  when specifying  $\Phi$ . Secondly, the estimates of  $\Phi$  are intended for use in a simple Bowen ratio framework for specifying satellite latent heat (Mallick et al., 2014b) and we believe it to be important that the complexity of the methods used here are commensurate with those used in the simple Bowen ratio approach. Related to this, we have tried to restrict the approach to largely using only AIRS data which provides the satellite soundings required for the Bowen ratio estimates. This single platform approach is to ensure the estimates do not suffer unduly from blending different data sources. Finally, complex radiative transfer approaches are also prone to the effects of significant uncertainties (Betts et al., 1993; Morcrette, 2002; Seidel et al., 2010).

## 5 Conclusions

We have only evaluated the satellite retrievals using data from terrestrial sites, and clearly it would be worthwhile repeating this for the ocean retrievals if possible. We have held back on this evaluation here because of the lack of an extensive network of instantaneous latent and sensible heat flux or radiative flux data over the oceans, although we note that the SEAFLEX project within the Global Energy and Water Experiment (GEWEX) initiative should give rise to such a database in the near future. From the terrestrial evaluation we would argue that the methodology employed here shows some promise for specifying both  $R_N$  and  $\Phi$ , although the results suggest the need for improvements particularly in the specification of  $R_{S\downarrow}$ . More detailed studies evaluating the representativeness of each tower site footprint in relation to the  $1^\circ$  scale within which it is situated could prove useful in this regard as would methods for cloud-proofing the satellite retrievals under persistent cloudy sky conditions. Similarly, evaluation under extreme conditions (e.g. high altitudes and latitudes) is also required.

Having derived and provisionally evaluated  $\Phi$  for terrestrial systems this is available to schemes for estimating latent and sensible heat using satellite data. Given we have resorted to the minimal amount of calibration in deriving  $\Phi$  it would appear sensible if a similar philosophy were adopted in developing satellite-based schemes for these important fluxes. With the availability of high spatial and temporal resolution geostationary imager–sounder data from GOES and, in the near future, GIFTS (Geosynchronous Interferometric Fourier Transform Spectrometer) and INSAT (Indian National Satellite)-3D our present approach could be extended to derive  $\Phi$  at the half hour time scale. In addition to opportunities in specifying large scale surface heat and water vapour fluxes, the heat capacity estimates made here clearly carry information on variations in terrestrial properties such as surface moisture storage and we envisage that studies to develop this concept further could prove fruitful, particularly because of the emergence of satellite microwave data against which the results could be compared.

**BGD**

11, 11825–11861, 2014

### Components of near-surface energy balance derived from satellite soundings

K. Mallick et al.

Title Page

Abstract

Introduction

Conclusions

References

Tables

Figures

◀

▶

◀

▶

Back

Close

Full Screen / Esc

Printer-friendly Version

Interactive Discussion



*Acknowledgements.* We would like to acknowledge Goddard Earth Sciences–Data & Information Services Centre (GESS–DISC), Level 1 and Atmosphere Archive and Distribution System (LAADS) web interface, NASA, and for putting the AIRS and MODIS data into the public domain. We kindly acknowledge all the site PI’s who have provided terrestrial flux data through the FLUXNET data archive. The AmeriFlux regional network component of this archive is supported with funding from the US Department of Energy under its Terrestrial Carbon project.

## References

- Adhikari, L., Wang, Z., and Whiteman, D.: Cloudy assessment within an atmospheric infrared sounder pixel by combining moderate resolution spectroradiometer and atmospheric radiation measurement program ground-based Lidar and radar measurements, in: Sixteenth ARM Science Team Meeting Proceedings, Albuquerque, NM, 27–31 March, 1–8, 2006.
- Ammann, C., Flechard, C. R., Leifeld, J., Neftel, A., and Fuhrer, J.: The carbon budget of newly established temperature grassland depends on management intensity, *Agr. Ecosyst. Environ.*, 121, 5–20, 2007.
- Anderson, M. C., Allen, R. G., Morse, A., and Kustas, W. P.: Use of Landsat thermal imagery in monitoring evapotranspiration and managing water resources, *Remote Sens. Environ.*, 122, 50–65, 2012.
- Anthoni, P. M., Knohl, A., Rebmann, C., Freibauer, A., Mund, M., Ziegler, W., Kolle, O., and Schulze, E. D.: Forest and agricultural land-use-dependent CO<sub>2</sub> exchange in Thuringia, Germany, *Glob. Change Biol.*, 10, 2005–2019, 2004.
- Aubinet, M., Chermanne, B., Vandenhaute, M., Longdoz, B., Yernaux, M., and Laitat, F.: Long term carbon dioxide exchange above a mixed forest in the Belgian Ardennes, *Agr. Forest Meteorol.*, 108, 293–315, 2001.
- Aumann, H. H., Chahine, M. T., Gautier, C., Goldberg, M. D., Kalnay, E., McMillin, L. M., Revercomb, H., Rosenkranz, P. W., Smith, W. L., Staelin, D. H., Strow, L., L., and Susskind, J.: AIRS/AMSU/HSB on the aqua mission: design, science objectives, data products and processing systems, *IEEE T. Geosci. Remote*, 41, 253–264, 2003.
- Baker, J. M. and Baker, D. G.: Long-term ground heat flux and heat storage at a mid-latitude site, *Climatic Change*, 54, 295–303, 2002.

## Components of near-surface energy balance derived from satellite soundings

K. Mallick et al.

Title Page

Abstract

Introduction

Conclusions

References

Tables

Figures



Back

Close

Full Screen / Esc

Printer-friendly Version

Interactive Discussion



## Components of near-surface energy balance derived from satellite soundings

K. Mallick et al.

[Title Page](#)

[Abstract](#)

[Introduction](#)

[Conclusions](#)

[References](#)

[Tables](#)

[Figures](#)



[Back](#)

[Close](#)

[Full Screen / Esc](#)

[Printer-friendly Version](#)

[Interactive Discussion](#)



- Baldocchi, D. D., Falge, E., Gu, L., Olson, R., Hollinger, D., Running, S., Anthoni, P., Bernhofer, C., Davis, K., Evans, R., Fuentes, J., Goldstein, A., Katul, G., Law, B., Lee, X., Malhi, Y., Meyers, T., Munger, W., Oechel, W., Paw U, K. T., Pilegaard, K., Schmid, H. P., Valentini, R., Verma, S., Vesala, T., Wilson, K., and Wofsy, S.: Fluxnet: a new tool to study the temporal and spatial variability of ecosystem-scale carbon dioxide, water vapor, and energy flux densities, *B. Am. Meteorol. Soc.*, 82, 2415–2434, 2001.
- Baldocchi, D. D., Xu, L. K., and Kiang, N.: How plant functional-type, weather, seasonal drought, and soil physical properties alter water and energy fluxes of an oak-grass savanna and an annual grassland, *Agr. Forest Meteorol.*, 123, 13–39, 2004.
- Bastiaanssen, W. G. M., Menenti, M., Feddes, R. A., and Holtslag, A. A. M.: The Surface Energy Balance Algorithm for Land (SEBAL): Part 1 Formulation, *J. Hydrol.*, 212–213, 198–212, 1998.
- Batra, N., Islam, S., Venturini, V., Bisht, G., and Jiang, L.: Estimation and comparison of evapotranspiration from MODIS and AVHRR sensors for clear sky days over the southern great plains, *Remote Sens. Environ.*, 103, 1–15, 2006.
- Betts, A. K., Ball, J. H., and Beljaars, A. C. M.: Comparison between the land surface response of the ECMWF model and the FIFE-1987 data, *Q. J. Roy. Meteor. Soc.*, 119, 975–1001, 1993.
- Bindi, M., Miglietta, F., and Zipoli, G.: Different methods for separating diffuse and direct components of solar radiation and their application in crop growth models, *Climate Res.*, 2, 47–54, 1992.
- Bisht, G. and Bras, R.: Estimation of net radiation from the MODIS data under all sky conditions: Southern Great Plains case study, *Remote Sens. Environ.*, 114, 1522–1534, 2010.
- Bisht, G. and Bras, R.: Estimation of net radiation from the Moderate Resolution Imaging Spectroradiometer over the Continental United States, *IEEE T. Geosci. Remote*, 49, 2448–2462, doi:10.1109/TGRS.2010.2096227, 2011.
- Bisht, G., Venturini, V., Islam, S., and Jiang, L.: Estimation of net radiation using MODIS (Moderate Resolution Imaging Spectroradiometer) Terra data for clear sky days, *Remote Sens. Environ.*, 97, 52–67, 2005.
- Bounoua, L., Hall, F. G., Sellers, P. J., Kumar, A., Collatz, G. J., Tucker, C. J., and Imhoff, M. L.: Quantifying the negative feedback of vegetation to greenhouse warming: a modeling approach, *Geophys. Res. Lett.*, 37, L23701, doi:10.1029/2010GL045338, 2010.

## Components of near-surface energy balance derived from satellite soundings

K. Mallick et al.

[Title Page](#)

[Abstract](#)

[Introduction](#)

[Conclusions](#)

[References](#)

[Tables](#)

[Figures](#)

[⏪](#)

[⏩](#)

[◀](#)

[▶](#)

[Back](#)

[Close](#)

[Full Screen / Esc](#)

[Printer-friendly Version](#)

[Interactive Discussion](#)



Cai, G., Xue, Y., Hu, Y., Guo, J., Wang, Y., and Qi, S.: Quantitative study of net radiation from MODIS data in the lower boundary layer in Poyang Lake area of Jiangxi Province, China, *Int. J. Remote Sens.*, 28, 4381–4389, 2007.

Cano, D., Monget, J. M., Albuissou, M., Guillard, H., Regas, N., and Wald, L.: A method for the determination of the global solar radiation from meteorological satellite data, *Sol. Energy*, 37, 31–39, 1986.

Carswell, F. E., Costa, A. L., Palheta, M., Malhi, Y., Meir, P., Costa, J. D. R., Ruivo, M. D., Leal, L. D. M., Costa, J. M. N., Clement, R. J., and Grace, J.: Seasonality in CO<sub>2</sub> and H<sub>2</sub>O flux at an eastern Amazonian rain forest, *J. Geophys. Res.-Atmos.*, 107, 8076, doi:10.1029/2000JD000284, 2002.

Chen, X., Huang, X., Loeb, N. G., and Wei, H.: Comparisons of clear-sky outgoing far-IR flux inferred from satellite observations and computed from the three most recent reanalysis products, *J. Climate*, 26, 478–494, doi:10.1175/JCLI-D-1200212.1, 2013.

Choudhury, B. J.: Relationships between vegetation indices, radiation absorption, and net photosynthesis evaluated by a sensitivity analysis, *Remote Sens. Environ.*, 22, 209–233, 1987.

Choudhury, B. J.: Estimating gross photosynthesis using satellite and ancillary data: approach and preliminary results, *Remote Sens. Environ.*, 75, 1–21, 2001.

Cook, B. D., Davis, K. J., Wang, W., Desai, A., Berger, B. W., Teclaw, R. M., Martin, J. G., Bolstad, P. V., Bakwin, P. S., Yi, C., and Heilman, W.: Carbon exchange and venting anomalies in an upland deciduous forest in northern Wisconsin, USA, *Agr. Forest Meteorol.*, 126, 271–295, 2004.

Corbari, C., Sobrino, J. A., Mancini, M., and Hidalgo, V.: Land surface temperature representativeness in a heterogeneous area through a distributed energy-water balance model and remote sensing data, *Hydrol. Earth Syst. Sci.*, 14, 2141–2151, doi:10.5194/hess-14-2141-2010, 2010.

de Araújo, A. C., Nobre, A. D., Kruijt, B., Elbers, J. A., Dallarosa, R., Stefani, P., von Randow, C., Manzi, A. O., Culf, A. D., Gash, J. H. C., Valentini, R., and Kabat, P.: Comparative measurements of carbon dioxide fluxes from two nearby towers in a central Amazonian rainforest: the Manaus LBA site, *J. Geophys. Res.-Atmos.*, 107, 8090, doi:10.1029/2001JD000676, 2002.

Dubayah, R. and Loechel, S.: Modeling topographic solar radiation using GOES data, *J. Appl. Meteorol.*, 36, 141–154, 1997.

## Components of near-surface energy balance derived from satellite soundings

K. Mallick et al.

Title Page

Abstract

Introduction

Conclusions

References

Tables

Figures

◀

▶

◀

▶

Back

Close

Full Screen / Esc

Printer-friendly Version

Interactive Discussion



Fischer, M. L., Billesbach, D. P., Berry, J. A., Riley, W. J., and Torn, M. S.: Spatiotemporal variations in growing season exchanges of CO<sub>2</sub>, H<sub>2</sub>O, and sensible heat in agricultural fields of the Southern Great Plains, *Earth Int.*, 11, 1–21, 2007.

Foken, T.: The energy balance closure problem: an overview, *Ecol. Appl.*, 18, 1351–1367, 2008.

Foken, T., Wimmer, F., Mauder, M., Thomas, C., and Liebethal, C.: Some aspects of the energy balance closure problem, *Atmos. Chem. Phys.*, 6, 4395–4402, doi:10.5194/acp-6-4395-2006, 2006.

Fouquart, Y. and Bonnel, B.: Computations of solar heating of the Earth's atmosphere: a new parameterization, *Beitr. Phys. Atmos.*, 53, 35–62, 1980.

Gao, J. and Wu, S.: Simulated effects of land cover conversion on the surface energy budget in the Southwest of China, *Energies*, 7, 1251–1264, doi:10.3390/en7031251, 2014.

Gao, W., Coulter, R. L., Lesht, B. M., Qiu, J., and Wesely, M. L.: Estimating clear-sky regional surface fluxes in the southern great plains atmospheric radiation measurement site with ground measurements and satellite observations, *J. Appl. Meteorol.*, 37, 5–22, 1998.

Giambelluca, T. W., Hölscher, D., Bastos, T. X., Frazão, R. R., Nullet, M. A., and Zeigler, A. D.: Observations of albedo and radiation balance over postforest land surfaces in the eastern Amazon Basin, *J. Climate*, 10, 919–928, 1997.

Gilmanov, T. G., Soussana, J. F., Aires, L., Allard, V., Ammann, C., Balzarolo, M., Barcza, Z., Bernhofer, C., Campbell, C. L., Cernusca, A., Cescatti, A., Brown, J. C., Dirks, O. M., Dore, S., Eugster, W., Fuhrer, J., Gimeno, C., Gruenwald, T., Haszpra, L., Hensen, A., Ibrom, A., Jacobs, A. F. G., Jones, M. B., Lanigan, G., Laurila, T., Ohila, A., Manca, G., Marcolla, B., Nagy, Z., Pilegaard, K., Pinter, K., Pio, C., Raschi, A., Rogiers, N., Sanz, M. J., Stefani, P., Sutton, M., Tuba, Z., Valentini, R., Williams, M. L., and Wohlfahrt, G.: Partitioning European grassland net ecosystem CO<sub>2</sub> exchange into gross primary productivity and ecosystem respiration using light response function analysis, *Agr. Ecosyst. Environ.*, 121, 93–120, 2007.

Goldstein, A. H., Hultman, N. E., Fracheboud, J. M., Bauer, M. R., Panek, J. A., Xu, M., Qi, Y., Guenther, A. B., and Baugh, W.: Effects of climate variability on the carbon dioxide, water, and sensible heat fluxes above a ponderosa pine plantation in the Sierra Nevada (CA), *Agr. Forest Meteorol.*, 101, 113–129, 2000.

Gough, C. M., Flower, C. E., Vogel, C. S., Dragoni, D., and Curtis, P. S.: Whole-ecosystem labile carbon production in a north temperate deciduous forest, *Agr. Forest Meteorol.*, 149, 1531–1540, 2009.

## Components of near-surface energy balance derived from satellite soundings

K. Mallick et al.

Title Page

Abstract

Introduction

Conclusions

References

Tables

Figures



Back

Close

Full Screen / Esc

Printer-friendly Version

Interactive Discussion



Goulden, M. L., Miller, S. D., da Rocha, H. R., Menton, M. C., De Freitas, H. C., Figuera, A. M. E. S., and De Sousa, C. A. D.: Diel and seasonal patterns of tropical forest CO<sub>2</sub> exchange, *Ecol. Appl.*, 14, S42–S54, 2004.

Granier, A., Loustau, D., and Breda, N.: A generic model of forest canopy conductance dependent on climate, soil water availability and leaf area index, *Ann. Forest Sci.*, 57, 755–765, 2000a.

Granier, A., Biron, P., and Lemoine, D.: Water balance, transpiration and canopy conductance in two beech stands, *Agr. Forest Meteorol.*, 100, 291–308, 2000b.

Gubler, S., Gruber, S., and Purves, R. S.: Uncertainties of parameterized surface downward clear-sky shortwave and all-sky longwave radiation., *Atmos. Chem. Phys.*, 12, 5077–5098, doi:10.5194/acp-12-5077-2012, 2012.

Hammerle, A., Haslwanter, A., Tappeiner, U., Cernusca, A., and Wohlfahrt, G.: Leaf area controls on energy partitioning of a temperate mountain grassland, *Biogeosciences*, 5, 421–431, doi:10.5194/bg-5-421-2008, 2008.

Hearty, T. J., Savtchenko, A., Tian, B., Fetzer, E., Yung, Y. L., Theobald, M., Vollmer, B., Fishbein, E., and Won, Y.: Estimating sampling biases and measurement uncertainties of AIRS/AMSU – a temperature and water vapor observations using MERRA reanalysis, *J. Geophys. Res.-Atmos.*, 119, 2725–2741, doi:10.1002/2013JD021205, 2014.

Heitman, J. L., Horton, R., Sauer, T. J., Ren, T. S., and Xiao, X.: Latent heat in soil heat flux measurements, *Agr. Forest Meteorol.*, 150, 1147–1153, 2010.

Hildebrandt, A., Afi, M. A., Amerjeed, M., Shammass, M., and Eltahir, E. A. B.: Ecohydrology of a seasonal cloud forest in Dhofar: 1. Field experiment, *Water Resour. Res.*, 43, W10411, doi:10.1029/2006WR005261, 2007.

Hirano, T., Hirata, R., Fujinuma, Y., Saigusa, N., Yamamoto, S., Harazono, Y., Takada, M., Inukai, K., and Inoue, G.: CO<sub>2</sub> and water vapor exchange of a larch forest in northern Japan, *Tellus B*, 55, 244–257, 2003.

Hirano, T., Segah, H., Harada, T., Limin, S., June, T., Hirata, R., and Osaki, M.: Carbon dioxide balance of a tropical peat swamp forest in Kalimantan, Indonesia, *Glob. Change Biol.*, 13, 412–425, 2007.

Hollinger, D. Y., Goltz, S. M., Davidson, E. A., Lee, J. T., Tu, K., and Valentine, H. T.: Seasonal patterns and environmental control of carbon dioxide and water vapour exchange in an ecotonal boreal forest, *Glob. Change Biol.*, 5, 891–902, 1999.

**Components of near-surface energy balance derived from satellite soundings**

K. Mallick et al.

[Title Page](#)[Abstract](#)[Introduction](#)[Conclusions](#)[References](#)[Tables](#)[Figures](#)[⏪](#)[⏩](#)[◀](#)[▶](#)[Back](#)[Close](#)[Full Screen / Esc](#)[Printer-friendly Version](#)[Interactive Discussion](#)

- Hou, J., Jia, G., Zhao, T., Wang, H., and Tang, B.: Satellite based estimation of daily average net radiation under clear sky conditions, *Adv. Atmos. Sci.*, 31, 705–720, 2014.
- Hsieh, C. I., Huang, C. W., and Kiely, G.: Long term estimation of soil heat flux by single layer soil temperature, *Int. J. Biometeorol.*, 53, 113–123, 2009.
- 5 Humes, K. S., Kustas, W. P., and Moran, M. S.: Use of remote sensing and reference site measurements to estimate instantaneous surface energy balance components over a semiarid rangeland watershed, *Water Resour. Res.*, 30, 1363–1373, 1994.
- Hutyra, L. R., Munger, J. W., Saleska, S. R., Gottlieb, E., Daube, B. C., Dunn, A. L., Amaral, D. F., de Camargo, P. B., and Wofsy, S. C.: Seasonal controls on the exchange of carbon and water in an Amazonian rain forest, *J. Geophys. Res.*, 112, G03008, doi:10.1029/2006JG000365, 2007.
- 10 Hwang, K., Choi, M., Lee, S. O., and Seo, J.-W.: Estimation of instantaneous and daily net radiation from MODIS data under clear sky conditions: a case study in East Asia, *Irrig. Sci.*, 31, 1173–1184, doi:10.1007/s00271-012-0396-3, 2013.
- 15 Jacobs, J. M., Anderson, M. C., Friess, L. C., and Diak, G. R.: Solar radiation, longwave radiation and eme, 49, 461–176, 2004.
- Jaksic, V., Kiely, G., Albertson, J., Katul, G., and Oren, R.: Net ecosystem exchange of grassland in contrasting wet and dry years, *Agr. Forest Meteorol.*, 139, 323–334, 2006.
- Jin, Z., Charlock, T. P., Smith Jr., W. L., and Rutledge, K.: A parameterization of ocean surface albedo, *Geophys. Res. Lett.*, 31, L22301, doi:10.1029/2004GL021180, 2004.
- 20 Katul, G. G., Leuning, R., and Oren, R.: Relationship between plant hydraulic and biochemical properties derived from a steady-state coupled water and carbon transport model, *Plant Cell Environ.*, 26, 339–350, 2003.
- Kaufmann, Y. J. and Koran, I.: Smoke and pollution aerosol effect on cloud cover, *Science*, 313, 655–658, 2006.
- 25 Kergoat, L., Grippa, M., Baille, A., Eymard, L., Lacaze, R., Mougín, E., Ottlé, C., Pellarin, T., Polcher, J., de Rosnay, P., Roujean, J.-L., Sandholt, I., Taylor, C. M., Zin, I., and Zribi, M.: Remote sensing of the land surface during the African Monsoon Multidisciplinary Analysis (AMMA), *Atmos. Sci. Lett.*, 12, 129–134, 2011.
- 30 Kustas, W. P. and Norman, J. M.: Evaluating the effects of subpixel heterogeneity on pixel average fluxes, *Remote Sens. Environ.*, 74, 327–342, 2000.
- Lakshmi, V. and Zehrhuhs, D.: Normalization and comparison of surface temperatures across a range of scales, *IEEE T. Geosci. Remote*, 40, 2636–2646, 2002.



**Components of near-surface energy balance derived from satellite soundings**

K. Mallick et al.

[Title Page](#)[Abstract](#)[Introduction](#)[Conclusions](#)[References](#)[Tables](#)[Figures](#)[Back](#)[Close](#)[Full Screen / Esc](#)[Printer-friendly Version](#)[Interactive Discussion](#)

- Li, J. and Islam, S.: On the estimation of soil moisture profile and surface fluxes partitioning from sequential assimilation of surface layer soil moisture, *J. Hydrol.*, 220, 86–103, 1999.
- Liang, S., Strahler, A. H., and Walthall, C.: Retrieval of land surface albedo from satellite observations: a simulation study, *J. Appl. Meteorol.*, 38, 712–725, 1999.
- 5 Liang, S., Shuey, C., Russ, A., Fang, H., Chen, M., Walthall, C., and Daughtry, C.: Narrowband to broadband conversions of land surface albedo: II. Validation, *Remote Sens. Environ.*, 84, 25–41, 2002.
- Liang, X., Wood, E. F., Lettenmaier, D. P., Lohmann, D., Boone, A., Chang, S., Chen, F., Dai, Y., Desborough, C., Dickinson, R. F., Duan, Q., Ek, M., Gusev, Y. M., Habets, F., Irannejad, P.,  
10 Koster, R., Mitchell, K. E., Nasonova, O. N., Noilhan, J., Schaake, J., Schlosser, A., Shao, Y., Shmakin, A. B., Verseghy, D., Warrach, K., Wetzel, P., Xue, Y., Yang, Z. - L., and Zeng, Q.: The Project for Intercomparison of Land-surface Parameterization Schemes (PILPS) phase 2 (c) Red-Arkansas River basin experiment: 2. Spatial and temporal analysis of energy fluxes, *Global Planet. Change*, 19, 137–159, 1998.
- 15 Lin, B., Stackhouse Jr., P. W., Minnis, P., Wielicki, B. A., Hu, Y., Sun, W., Fan, T.-F., and Hinkelman, L. M.: Assessment of global annual atmospheric energy balance from satellite observations, *J. Geophys. Res.*, 113, D16114, doi:10.1029/2008JD009869, 2008.
- Liu, Z., Vavrus, S., He, F., Wen, N., and Zhong, Y.: Rethinking tropical ocean response to global warming: the enhanced equatorial warming, *J. Climate*, 18, 4684–4700, 2005.
- 20 Ma, Y., Su, Z., Li, Z., Koike, T., and Menenti, M.: Determination of regional net radiation and soil heat flux over a heterogeneous landscape of the Tibetan Plateau, *Hydrol. Process.*, 16, 2963–2971, 2002.
- Mallick, K., Bhattacharya, B. K., Rao, V. U. M., Reddy, D. R., Banerjee, S., Hoshali, V., Pandey, V., Kar, G., Mukherjee, J., Vyas, S. P., Gadgil, A. S., and Patel, N. K.: Latent heat flux estimation in clear sky days over Indian agroecosystems using noontime satellite remote sensing data, *Agr. Forest Meteorol.*, 149, 1646–1665, 2009.
- 25 Mallick, K., Jarvis, A. J., Boegh, E., Fisher, J. B., Drewry, D. T., Tu, K. P., Hook, S. J., Hulley, G., Ardo, J., Beringer, J., Arain, A., and Niyogi, D.: A surface temperature initiated closure (STIC) for surface energy balance fluxes, *Remote Sens. Environ.*, 141, 243–261, 2014a.
- 30 Mallick, K., Jarvis, A., Wohlfahrt, G., Kiely, G., Hirano, T., Miyata, A., Yamamoto, S., and Hoffmann, L.: Components of near-surface energy balance derived from satellite soundings – Part 2: Latent heat flux, *Biogeosciences Discuss.*, 11, 8085–8113, doi:10.5194/bgd-11-8085-2014, 2014b.



## Components of near-surface energy balance derived from satellite soundings

K. Mallick et al.

[Title Page](#)

[Abstract](#)

[Introduction](#)

[Conclusions](#)

[References](#)

[Tables](#)

[Figures](#)

[⏪](#)

[⏩](#)

[◀](#)

[▶](#)

[Back](#)

[Close](#)

[Full Screen / Esc](#)

[Printer-friendly Version](#)

[Interactive Discussion](#)



- Niemela, S., Raisanen, P., and Savijarvi, H.: Comparison of surface radiative flux parameterizations, Part I: Longwave radiation, *Atmos. Res.*, 58, 1–18, 2001.
- Ochsner, T. E., Sauer, T. J., and Horton, R.: Soil heat storage measurements in energy balance studies, *Agron. J.*, 99, 311–319, 2007.
- 5 Oliphant, A. J., Spronken-Smith, R. A., Sturman, A. P., and Owens, I. F.: Spatial variability of surface radiation fluxes in mountainous terrain, *J. Appl. Meteorol.*, 42, 113–128, 2003.
- Penman, H. L.: Natural evaporation from open water, bare soil and grass, *Proc. R. Soc. Lon. Ser.-A*, 193, 120–145, 1948.
- Pinker, R. T. and Laszlo, I.: Modeling surface solar irradiance for satellite applications on a global scale, *J. Appl. Meteorol.*, 31, 194–211, 1992.
- 10 Prata, A. J.: A new long-wave formula for estimating downward clear-sky radiation at the surface, *Q. J. Roy. Meteor. Soc.*, 122, 1127–1151, 1996.
- Priestley, K. J., Smith, G. L., Thomas, S., Cooper, D., Lee, R. B., Walikainen, D., Hess, P., Szewczyk, Z. P., and Wilson, R.: Radiometric performance of the CERES Earth radiation budget climate record sensors on the EOS Aqua and Terra Spacecraft through April 2007, *J. Atmos. Ocean. Tech.*, 28, 3–21, doi:10.1175/2010JTECHA1521.1, 2011.
- 15 Quaas, J., Stevens, B., Stier, P., and Lohmann, U.: Interpreting the cloud cover – aerosol optical depth relationship found in satellite data using a general circulation model, *Atmos. Chem. Phys.*, 10, 6129–6135, doi:10.5194/acp-10-6129-2010, 2010.
- 20 Reichstein, M., Tenhunen, J., Rouspard, O., Ourcival, J. M., Rambal, S., Miglietta, F., Peressotti, A., Pecchiari, M., Tirone, G., and Valentini, R.: Inverse modeling of seasonal drought effects on canopy CO<sub>2</sub>/H<sub>2</sub>O exchange in three Mediterranean ecosystems, *J. Geophys. Res.-Atmos.*, 108, 4726, doi:10.1029/2003JD003430, 2003.
- Ryu, Y., Kang, S., Moon, S. K., and Kim, J.: Evaluation of land surface radiation balance derived from moderate resolution imaging spectroradiometer (MODIS) over complex terrain and heterogeneous landscape on clear sky days, *Agr. Forest Meteorol.*, 148, 1538–1552, 2008.
- 25 Saigusa, N., Yamamoto, S., Murayama, S., Kondo, H., and Nishimura, N.: Gross primary production and net ecosystem exchange of a cool-temperate deciduous forest estimated by the eddy covariance method, *Agr. Forest Meteorol.*, 112, 203–215, 2002.
- 30 Saito, M., Miyata, A., Nagai, H., and Yamada, T.: Seasonal variation of carbon dioxide exchange in rice paddy field in Japan, *Agr. Forest Meteorol.*, 135, 93–109, 2005.

## Components of near-surface energy balance derived from satellite soundings

K. Mallick et al.

Title Page

Abstract

Introduction

Conclusions

References

Tables

Figures

◀

▶

◀

▶

Back

Close

Full Screen / Esc

Printer-friendly Version

Interactive Discussion



- Salomon, J. G., Schaff, C. B., Strahler, A. H., Gao, F., and Jin, Y. F.: Validation of the MODIS bidirectional reflectance distribution function and albedo retrievals using combined observations from the Aqua and Terra platforms, *IEEE T. Geosci. Remote*, 44, 1555–1565, 2006.
- Santanello Jr., J. A. and Friedl, M. A.: Diurnal covariation in soil heat flux and net radiation, *J. Appl. Meteorol.*, 42, 851–862, 2003.
- Sauer, T. J. and Horton, R.: Soil heat flux, in: *Micrometeorology in Agricultural Systems*, edited by: Hatfield, J. L. and Baker, J. M., American Society of Agronomy, Madison, Wisconsin, USA, 131–154, 2005.
- Scholes, R. J., Gureja, N., Giannecchini, M., Dovie, D., Wilson, B., Davidson, N., Piggott, K., McLoughlin, C., van der Velde, K., Freeman, A., Bradley, S., Smart, R., and Ndala, S.: The environment and vegetation of the flux measurement site near Skukuza, Kruger National Park, *Koedoe*, 44, 73–83, 2001.
- Schwartz, S. E.: Heat capacity, time constant, and sensitivity of Earth's climate system, *J. Geophys. Res.*, 112, D24S05, doi:10.1029/2007JD008746, 2007.
- Seidel, F. C., Kokhanovsky, A. A., and Schaepman, M. E.: Fast and simple model for atmospheric radiative transfer, *Atmos. Meas. Tech.*, 3, 1129–1141, doi:10.5194/amt-3-1129-2010, 2010.
- Stackhouse, P. W., Gupta, S. K., Cox, S. J., Chiacchio, M., and Mikovitz, J. C.: The WCRP/GEWEX Surface Radiation Budget Project Release 2: An assessment of surface fluxes at 1° resolution, in: *IRS 2000: Current Problems in Atmospheric Radiation*, edited by: Smith, W. L. and Timofeyev, Y. M., International Radiation Symposium, St. Petersburg, Russia, 24–29, 2000.
- Stephens, G. L., Wild, M., Stackhouse, P. W., L'Ecuyer, T., Kato, S., and Henderson, D. S.: The global character of the flux of downward longwave radiation, *J. Climate*, 25, 2329–2340, doi:10.1175/JCLI-D-11-00262.1, 2012.
- Stisen, S., Sandholt, I., Nørgaard, A., Fensholt, R., and Jensen, K. H.: Combining the triangle method with thermal inertia to estimate regional evapotranspiration applied to MSG-SEVIRI data in the Senegal river basin, *Remote Sens. Environ.*, 112, 1242–1255, 2008.
- Stramma, L., Cornillon, P., Weller, R. A., Price, J. F., and Briscoe, M. G.: Large diurnal sea surface temperature variability: satellite and in situ measurements, *J. Geophys. Res.*, 16, 827–837, 1986.

## Components of near-surface energy balance derived from satellite soundings

K. Mallick et al.

Title Page

Abstract

Introduction

Conclusions

References

Tables

Figures

◀

▶

◀

▶

Back

Close

Full Screen / Esc

Printer-friendly Version

Interactive Discussion



Sultan, S., Wu, R., and Ahmed, I.: Impact of terrain and cloud cover on the distribution of incoming direct solar radiation over Pakistan, *J. Geogr. Inf. Sys.*, 6, 70–77, doi:10.4236/jgis.2014.61008, 2014.

Tamai, K., Abe, T., Araki, M., and Ito, H.: Radiation budget, soil heat flux and latent heat flux at the forest floor in warm, temperate mixed forest, *Hydrol. Process.*, 12, 2105–2114, 1998.

Thornton, P. E. and Running, S. W.: An improved algorithm for estimating incident daily solar radiation from measurements of temperature, humidity, and precipitation, *Agr. Forest Meteorol.*, 93, 211–228, 1999.

Tittebrand, A. and Berger, F. H.: Spatial heterogeneity of satellite derived land surface parameters and energy flux densities for LITFASS-area, *Atmos. Chem. Phys.*, 9, 2075–2087, doi:10.5194/acp-9-2075-2009, 2009.

Trenberth, K.: Changes in precipitation with climate change, *Clim. Res.*, 47, 123–138, doi:10.3354/cr00953, 2011.

Trenberth, K., Fasullo, J., and Kiehl, J.: Earth's global energy budget, *B. Am. Meteorol. Soc.*, 90, 311–323, doi:10.1175/2008BAMS2634.1, 2009.

Urbanski, S., Barford, C., Wofsy, S., Kucharik, C., Pyle, E., Budney, J., Fitzjarrald, D., Czikowsky, M., and Munger, J. W.: Factors controlling CO<sub>2</sub> exchange at Harvard Forest on hourly to annual time scales, *J. Geophys. Res.*, 112, G02020, doi:10.1029/2006JG000293, 2007.

Verhoef, A., Otte, C., Cappelaere, B., Murray, T., Saux-Picart, S., Zribi, M., Maignan, F., Boulain, N., Demarty, J., and Ramier, D.: Spatio-temporal surface soil heat flux estimates from satellite data: results for the AMMA experiment at the Fakara (Niger) supersite, *Agr. Forest Meteorol.*, 154–155, 55–66, doi:10.1016/j.agrformet.2011.08.003, 2012.

Wielicki, B. A., Barkstrom, B. R., Baum, B. A., Charlock, T. P., Green, R. N., Kratz, D. P., Lee, R. B., Minnis, P., Smith, G. L., Wong, T. M., Young, D. F., Cess, R. D., Coakley, J. A., Crommelynck, D. A. H., Donner, L., Kandel, R., King, M. D., Miller, A. J., Ramanathan, V., Randall, D. A., Stowe, L. L., and Welch, R. M.: Clouds and the Earth's Radiant Energy System (CERES): algorithm overview, *IEEE T. Geosci. Remote*, 36, 1127–1141, 1998.

Wild, M., Folini, D., Schar, C., Loeb, N., Dutton, E. G., and Langlo, G. K.: The global energy balance from a surface perspective, *Clim. Dynam.*, 40, 3107–3134, doi:10.1007/s00382-012-1569-8, 2013.

Wilson, K. B., Goldstein, A. H., Falge, E., Aubinet, M., Baldocchi, D., Berbigier, P., Bernhofer, Ch., Ceulemans, R., Dolman, H., Field, C., Grelle, A., Law, B., Meyers, T., Moncrieff, J.,



## Components of near-surface energy balance derived from satellite soundings

K. Mallick et al.

[Title Page](#)

[Abstract](#)

[Introduction](#)

[Conclusions](#)

[References](#)

[Tables](#)

[Figures](#)

[◀](#)

[▶](#)

[◀](#)

[▶](#)

[Back](#)

[Close](#)

[Full Screen / Esc](#)

[Printer-friendly Version](#)

[Interactive Discussion](#)



**Table 1.** Eddy covariance sites used for the evaluation of the satellite derived  $R_N$  and  $\Phi$ .

Biome type	Site name, Country	Latitude	Longitude	Reference
Evergreen broadleaf forest (EBF)	Palagkaraya, Indonesia	-2.35	114.04	Hirano et al. (2007)
	Puechabon, France	43.74	3.6	Reichstein et al. (2003)
	Caxiuana Forest-Almeirim, Brazil	-1.72	-51.46	Carswell et al. (2002)
	Manaus – ZF2 K34, Brazil	-2.61	-60.21	de Araújo et al. (2004)
	Santarem-Km67, Brazil	-2.86	-54.96	Hutyra et al. (2007)
	Santarem-Km83, Brazil	-3.02	-54.58	Goulden et al. (2004)
Mixed forest (MF)	Vielsalm, Belgium	50.31	5.99	Aubinet et al. (2001)
	Tomakomai National forest, Japan	42.73	141.52	Hirano et al. (2003)
	Changbaishan, China	42.4	128.09	Zhang et al. (2006)
Grassland (GRA)	Oensingen1 grass, Switzerland	47.29	7.73	Ammann et al. (2007)
	Neustift/Stubai Valley, Austria	47.12	11.32	Hammerle et al. (2008)
	Goodwin Creek, USA	34.25	-89.87	unpublished data
	Bugacpuszta, Hungary	46.69	19.61	Gilmanov et al. (2007)
Cropland (CRO)	Dripsey, Ireland	51.99	-8.75	Jaksic et al. (2006)
	ARM Southern Great Plains, USA	36.61	-97.49	Fischer et al. (2007)
	Bondville, USA	40.01	88.29	Meyers et al. (2004)
Evergreen needleleaf forest (ENF)	Tsukuba, Japan	36.05	140.03	Saito et al. (2005)
	Le Bray, France	44.72	-0.77	Granier et al. (2000a)
	Duke Forest – loblolly pine, USA	35.98	-79.09	Katul et al. (2003)
	Blodgett forest, USA	38.89	-120.63	Goldstein et al. (2000)
Deciduous broadleaf forest (DBF)	Howland forest, USA	45.2	-68.74	Hollinger et al. (1999)
	Harvard Forest EMS Tower (HFR1), USA	42.54	-72.17	Urbanski et al. (2007)
	Univ. of Michigan Biological Station, USA	45.56	-84.71	Gough et al. (2009)
	Willow Creek, USA	45.81	-90.08	Cook et al. (2004)
	Hesse Forest – Sarrebourg, France	48.67	7.06	Granier et al. (2000b)
	Hainich, Germany	51.08	10.45	Anthoni et al. (2004)
	Morgan Monroe State forest, USA	39.32	-86.41	Baldocchi et al. (2001)
Savanna (SAV)	Takayama, Japan	36.15	137.42	Saigusa et al. (2002)
	Tonzi Ranch, USA	38.43	-120.97	Baldocchi et al. (2004)
	Skukuza, South Africa	-25.02	31.49	Scholes et al. (2001)

## Components of near-surface energy balance derived from satellite soundings

K. Mallick et al.

[Title Page](#)

[Abstract](#)

[Introduction](#)

[Conclusions](#)

[References](#)

[Tables](#)

[Figures](#)

[⏪](#)

[⏩](#)

[◀](#)

[▶](#)

[Back](#)

[Close](#)

[Full Screen / Esc](#)

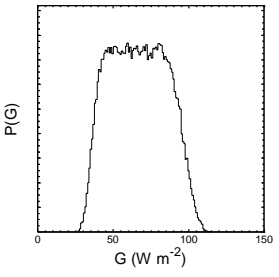
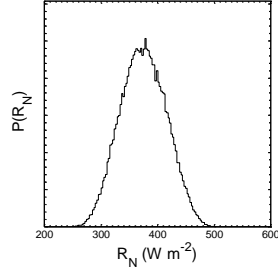
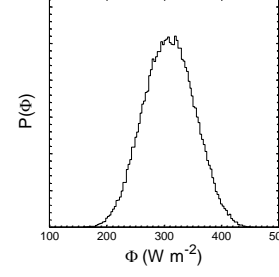
[Printer-friendly Version](#)

[Interactive Discussion](#)

**Table 2.** Sensitivity analysis results. The forcing data are taken for mid-summer on the Southern Great Plains, US. Sensitivities are locally linear, averaged across the ensemble response and expressed as dimensionless relative changes. Only absolute sensitivities  $> 0.1$  are shown.  $N = 10^5$  realisations.

		$G$ ( $\text{W m}^{-2}$ )	$R_N$ ( $\text{W m}^{-2}$ )	$\Phi$ ( $\text{W m}^{-2}$ )
$x$	sample range	$dG/dx$	$dR_N/dx$	$d\Phi/dx$
$\tau_A$	$\pm 10\%$	–	1.30	1.58
$f$	$\pm 10\%$	–	–0.77	–0.94
$\alpha$	$\pm 10\%$	–	–0.25	–0.31
$\varepsilon_S$	$\pm 10\%$	1.00	–0.31	–0.37
$\varepsilon_C$	$\pm 10\%$	–4.60	0.98	1.19
$T_S$	$\pm 1$ K	0.75	–0.17	–0.21
$T_{1000}$	$\pm 1$ K	–0.33	–	–

			
standard deviation	$18 \text{ W m}^{-2}$	$40 \text{ W m}^{-2}$	$44 \text{ W m}^{-2}$



## Components of near-surface energy balance derived from satellite soundings

K. Mallick et al.

Title Page

Abstract

Introduction

Conclusions

References

Tables

Figures

⏪

⏩

◀

▶

Back

Close

Full Screen / Esc

Printer-friendly Version

Interactive Discussion



**Table 3.** Comparative statistics for the satellite and tower derived  $R_N$  and  $\Phi$  for a range of biomes. Values in parenthesis are  $\pm$  one standard deviation.

Biome	$R_N$					$\Phi$				
	RMSD ( $\text{W m}^{-2}$ )	Gain	Offset	$r$	$N$	RMSD ( $\text{W m}^{-2}$ )	Gain	Offset	$r$	$N$
EBF	126.67	0.58 ( $\pm 0.08$ )	107.45 ( $\pm 39.93$ )	0.65 ( $\pm 0.09$ )	69	87.67	0.66 ( $\pm 0.08$ )	108.71 ( $\pm 32.10$ )	0.70 ( $\pm 0.09$ )	65
MF	104.21	0.82 ( $\pm 0.07$ )	-32.40 ( $\pm 23.73$ )	0.89 ( $\pm 0.08$ )	36	87.29	0.97 ( $\pm 0.10$ )	-65.25 ( $\pm 27.07$ )	0.86 ( $\pm 0.09$ )	32
GRA	74.29	0.73 ( $\pm 0.05$ )	51.37 ( $\pm 15.88$ )	0.88 ( $\pm 0.06$ )	59	61.51	0.83 ( $\pm 0.07$ )	15.71 ( $\pm 16.21$ )	0.86 ( $\pm 0.07$ )	53
CRO	89.13	0.73 ( $\pm 0.08$ )	35.62 ( $\pm 28.57$ )	0.84 ( $\pm 0.09$ )	36	53.31	0.99 ( $\pm 0.10$ )	-0.23 ( $\pm 23.98$ )	0.87 ( $\pm 0.09$ )	36
ENF	85.45	0.87 ( $\pm 0.04$ )	-26.83 ( $\pm 14.78$ )	0.96 ( $\pm 0.04$ )	48	66.7	1.01 ( $\pm 0.05$ )	-56.56 ( $\pm 15.27$ )	0.95 ( $\pm 0.05$ )	46
DBF	92.77	0.71 ( $\pm 0.05$ )	21.74 ( $\pm 15.15$ )	0.85 ( $\pm 0.06$ )	84	71.57	0.88 ( $\pm 0.06$ )	-16.70 ( $\pm 14.23$ )	0.85 ( $\pm 0.06$ )	80
SAV	103.98	0.69 ( $\pm 0.08$ )	56.28 ( $\pm 36.08$ )	0.87 ( $\pm 0.11$ )	23	61.98	0.97 ( $\pm 0.11$ )	-14.42 ( $\pm 37.68$ )	0.88 ( $\pm 0.25$ )	23
Pooled	98.21	0.75 ( $\pm 0.02$ )	23.37 ( $\pm 8.20$ )	0.88 ( $\pm 0.03$ )	355	72.26	0.90 ( $\pm 0.03$ )	-2.43 ( $\pm 8.19$ )	0.87 ( $\pm 0.03$ )	335

EBF = Evergreen broadleaf forest, MF = Mixed forest, GRA = Grassland, CRO = Cropland, ENF = Evergreen needleleaf forest, DBF = Deciduous broadleaf forest, SAV = Savanna.

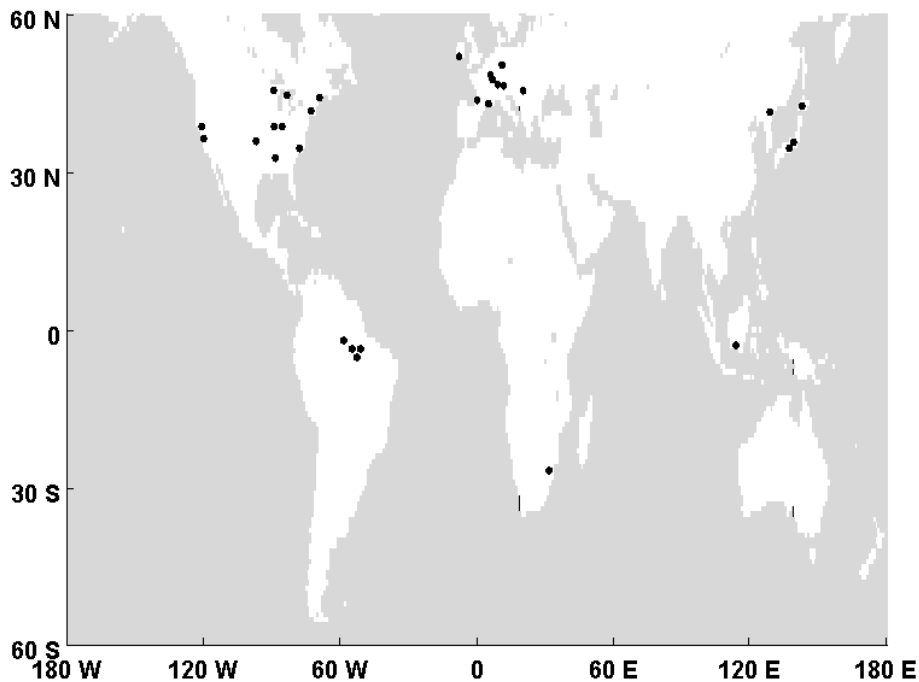


**Figure 1.** The distribution of the 30 eddy covariance tower sites used for evaluating  $R_N$  and  $\Phi$ .

## BGD

11, 11825–11861, 2014

### Components of near-surface energy balance derived from satellite soundings

K. Mallick et al.

[Title Page](#)

[Abstract](#)

[Introduction](#)

[Conclusions](#)

[References](#)

[Tables](#)

[Figures](#)



[Back](#)

[Close](#)

[Full Screen / Esc](#)

[Printer-friendly Version](#)

[Interactive Discussion](#)





## Components of near-surface energy balance derived from satellite soundings

K. Mallick et al.

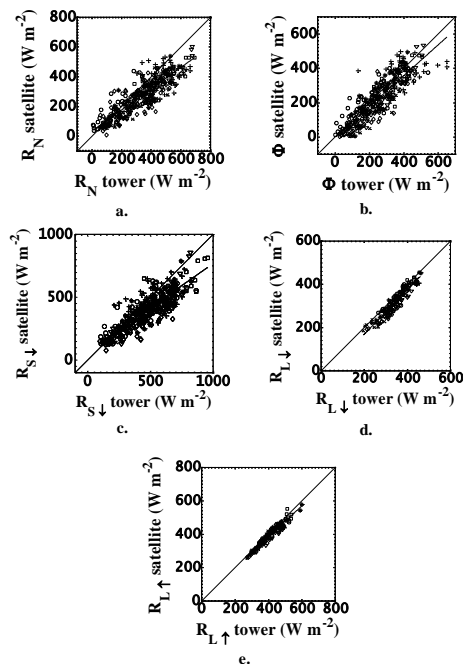


**Figure 3.** Comparison of satellite and tower monthly average 13:30LT (a)  $R_N$  and (b)  $\Phi$ . For details of the site characteristics see Table 1. For the comparative statistics see Table 2. The solid line is the pooled linear regression given in Table 2. Comparison of satellite and tower monthly average 13:30LT (c)  $R_{S\downarrow}$ , (d)  $R_{L\downarrow}$  and (e)  $R_{L\uparrow}$  for a selection of sites for which tower data for  $R_S$  (360 data points),  $R_{L\downarrow}$  (159 data points) and  $R_{L\uparrow}$  (159 data points) were available. The linear fit (solid line) between the two sources of  $R_S$  is,  $R_{S\downarrow}(\text{AIRS}) = 0.70 (\pm 0.02) R_{S\downarrow}(\text{tower}) + 67.68 (\pm 12.24)$ ;  $r = 0.84 (\pm 0.03)$ . The linear fit (solid line) between the two sources of  $R_{L\downarrow}$  is,  $R_{L\downarrow}(\text{AIRS}) = 1.03 (\pm 0.03) R_{L\downarrow}(\text{tower}) - 36.91 (\pm 10.05)$ ;  $r = 0.95 (\pm 0.03)$ . The linear fit (solid line) between the two sources of  $R_{L\uparrow}$  is,  $R_{L\uparrow}(\text{AIRS}) = 0.91 (\pm 0.02) R_{L\uparrow}(\text{tower}) + 20.43 (\pm 8.77)$ ;  $r = 0.96 (\pm 0.02)$ . The dashed lines are 1 : 1 in all cases.

(+ EBF; × MF; ○ GRA; \* CRO; ▽ ENF; ◇ DBF; □ SAV)

[Title Page](#)
[Abstract](#)
[Introduction](#)
[Conclusions](#)
[References](#)
[Tables](#)
[Figures](#)
[Back](#)
[Close](#)
[Full Screen / Esc](#)
[Printer-friendly Version](#)
[Interactive Discussion](#)


## Components of near-surface energy balance derived from satellite soundings

K. Mallick et al.

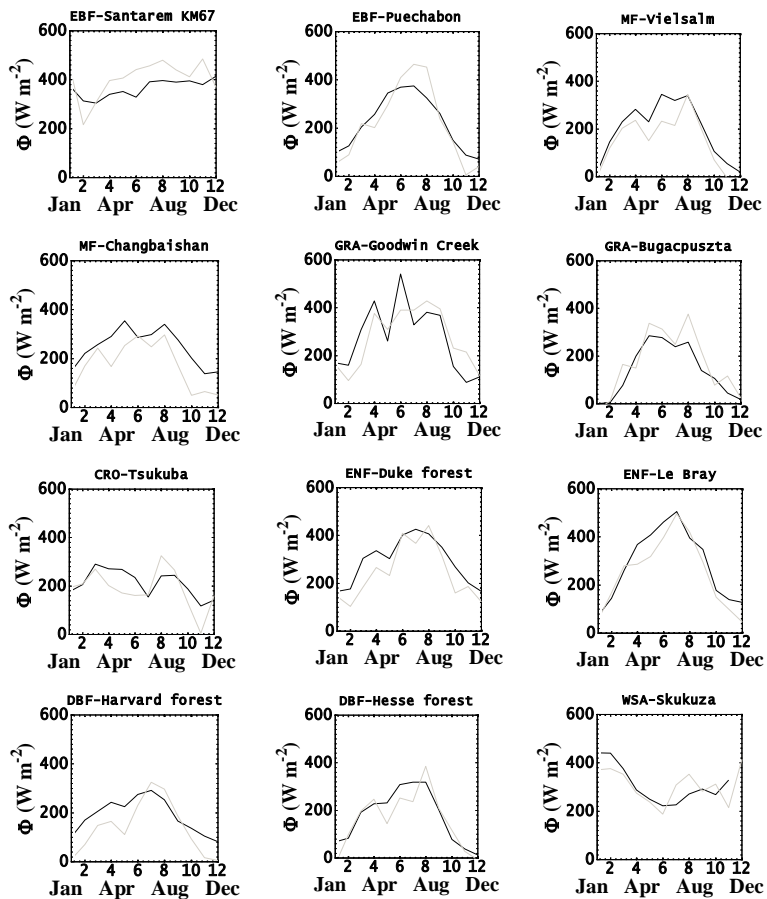


**Figure 4.** Satellite (grey) and tower (black) time series of monthly average 13:30 LT net available energy  $\Phi$  for a selection of sites for 2003.

Title Page

Abstract

Introduction

Conclusions

References

Tables

Figures

◀

▶

◀

▶

Back

Close

Full Screen / Esc

Printer-friendly Version

Interactive Discussion

